Sjournals
Scientific Journals
Scientific Journal of Review (2018) 7(1) 572-590
ISSN 2322-2433
doi: 10.14196/sjr.v7i1.2501

Contents lists available at Sjournals
Scientific Journal of **Review**
Journal homepage: www.sjournals.com

Original article

Optimization of heating characteristics of gas insulated switch-gear (GIS)

Muhammad Shahid Mastoi[a], Muhammad Shahzad Nazir[a,*], Muhammad Imran Chandia[b], Muhammad Shakeel Khosa[c], Hafiz Muhammad Jamsheed Nazir[d]

[a]*School of Electrical Power Engineering, South China University of Technology, Guangzhou, 510640, P.R. China.*
[b]*School of Automation Science and Engineering, South China University of Technology, Guangzhou, P.R. China.*
[c]*School Electrical and Electronic Engineering, North China Electric Power University, Beijing, P.R. China.*
[d]*School of Software Engineering, South China University of Technology, Guangzhou, P.R. China.*

*Corresponding author: epmsn_bhutta88@mail.scut.edu.cn

ARTICLE INFO

Article history,
Received 10 December 2017
Accepted 11 January 2018
Available online 18 January 2018
iThenticate screening 12 December 2017
English editing 10 January 2018
Quality control 17 January 2018

Keywords,
Gas insulated metal-enclosed switch-gear
Temperature rise analysis
GIS temperature field
Circuit breaker
Switch-gear
Optimization

ABSTRACT

Protection types of equipment are the mainstay of a power system. Recently, gas insulated metal-enclosed switch-gear (GIS) has developed the most important part of a power system protection. High-pressure gas insulated metal-enclosed switchgear may suffer overheating and can cause fatal accidents. The miniaturization and high performance of electrical equipment highlight the importance of thermal analysis. In this paper, the model simplification method of gas insulated metal-enclosed switchgear is studied and the complex structure of GIS is simplified according to the heat source of GIS. The heat source of GIS includes Joule heat of conductor and contact resistance heating. Furthermore, this paper considers the cooling effect of natural convection SF6. By employing the method of AC electromagnetic analysis and fluid-solid coupling analysis, harmonics under the effect of eddy current losses and the contact resistance method for the convection heat dissipation (for shell and air) have been selected. Finally, obtain the temperature distribution of gas insulated metal-enclosed switchgear. The simulation results are verified by temperature rise test. Thermal simulation analysis of gas insulated metal-enclosed switchgear is carried out, which can provide a theoretical and experimental reference for further research and design of improved protected products.

1. Introduction

Considering the increasing energy demand and multi systems of power generations attracted the industry and academia to provide the smooth and protected energy systems. Protection of every system is most desirable to avaid the undesirabel purturbations to enjoy the healthy efficient output (PD IEC-TS 62478, 2016; Nazir et al., 2017). Switchgear is a mechanical device, installed for the protection of power systems. It consists multi devices which are associated with control, metering and regulating of electric power system (Okubo and Yanabu, 2002; Shioiri et al., 1999). These devices in a logical manner are called switchgears. Switchgear refers various equipment associated with switching of electrical plants and circuit under the normal and abnormal operation. The types of switchgear depend upon the level of voltages. According to the voltage ratings, there are tri types, the low, medium and high voltage, which have up to 1 kV, 3 kV to 36 kV and up to 36 kV, respectively (Misrikhanov et al., 2003). Furthermore, the outdoor open terminal (switch yard), metal-enclosed, gas insulated metal-enclosed, compartment of GIS, design pressure of enclosure and gas insulated (Takahashi et al., 2005; Kuwahara et al., 1982) are the classifications of switchgears. A healthy GIS contains pre-assembled and tested units, corrosion resistance, need of minimal cleaning, low fault probability, operating life period, less requirement compares to AIS and miniaturization features (Qi et al., 2015; Ueta et al., 2014). The objective of this work is to develop an ANSYS based model of GIS, the calculation of heat transfer coefficient, DC-AC thermoelectric coupling simulation, GIS temperature rise test and hereinafter comprehensive comparison between simulation data and test data.

1.1. GIS material

The GIS technology is in a continuous development process involving new materials, technical functionality, manufacturing processes, quality, and reliability improvements (Zhang et al., 2000; Chmielewski et al., 2017). The result offers GIS with higher performances in voltage ratings (up to 1100 kV UHV systems), current ratings (up to 8000 A) and short circuit ratings (up to 100 kA) (Switchgear, High-voltage, 2001; Küchler, 2018). Meanwhile, the size, volume and cost of GIS have been reduced. This development is still continuing, however the steps are getting smaller in which the ratings are being increased or the size and volume is being reduced.

A constant development is carried out to investigate new technical principles like vacuum switching for high voltages 52 kV and above, alternatives to SF_6 for example, for insulating purposes in gas insulated transmission lines (GILs), electronic switching, or short circuit limitations (Riechert and Holaus, 2012; Xue et al., 2018). The basic materials to manufacture GIS are metals to form the enclosure and the conductors, epoxy resin insulating materials, insulating gas, contact materials for switches and breakers, and several metallic and insulator materials to fix and operate the GIS functionality. When invented in the 1960s the GIS materials were dominated by a steel enclosure, aluminum conductor, SF_6 insulating gas, and silver plated contact materials (Lee et al., 2011; Yanabu et al., 2002). In some cases, copper for the conductor was used to reduce the transmission losses of aluminum conductors. Later the enclosure material of the steel was replaced by aluminum alloys. The insulating gas SF_6 is still used because of its excellent performance of insulating high voltages with high reliability and its arc-quenching ability (Yanabu et al., 2002), which allows current ratings of up to 8000 A and short circuit ratings of up to 100 kA. Former gasses don't offer such features. The high global warming potential of SF_6 has been taken into account by developing a closed loop cycle for the lifetime of SF_6 which is fixed in international standards. The insulating materials are based on epoxy resin of various mixtures with additives for improvement of mechanical strength, tracking behavior and other properties to increase reliability. The basic materials are explained and their use in the GIS is described below.

1.2. Heat transfer coefficient

All the heat transfer processes in nature can be a general situation of heat conduction, heat convection and heat radiation (Riechert and Holaus, 2012; Xie et al., 2017). The heat transfer inside the switch cabinet is naturally no exception. The indoor part of the switch cabinet hand car room and the bus bar is mainly composed of a moving contact, a static contact, pressure terminal and a bus bar. Because of the friction and the contact force between the moving contact and the static contact, the moving contact and the static contact are the main heat source in the switch cabinet in the actual operation of the switch cabinet system. According to the second law of thermodynamics, heat transfer from high temperature to low temperature. Therefore, as the highest temperature parts, there is a thermal phenomenon from the contact to the surrounding parts. At the same time, the bus insulating layer and the external air flow between each other, so the convection process is also included.

Considering the above heat conduction and convection process, the main heat transfer process of the system is shown in Fig. 1.

From the above analysis, the heat transmits from the contact to the moving contact arm, the static contact arm, the insulation layer and the bus bar. Because of the existence of convection between the bus and the insulation layer, the heat convection process exists. Therefore, the heat transfer inside the switch cabinet is complicated multi-dimensional conduction and convection problem. For this kind of complex heat transfer process, the finite element method is used to construct the three-dimensional differential equation, but the solution is difficult because of this kind of boundary condition and the complicated model.

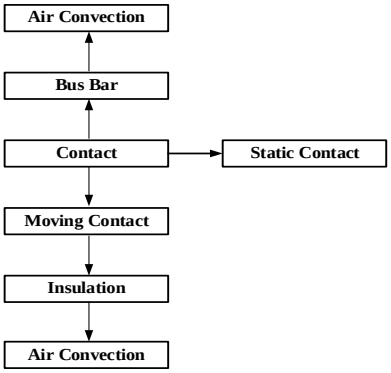

Fig. 1. Contact heat transfer flowchart.

Overall coefficient of heat transfer includes three heat dispatch methods. K_T can represent the ability of heat dispatch. The equation is called Newton cooling formula, as shown in Eq. 1.

$$P = K_T A\tau = K_T A(T\text{-}T_0) \quad (1)$$

Symbols in the equation are denoting:

P——total power loss;
A——valid area of dissipation;
τ——temperature rise of heat element;
T——is the heat element temperature and;
T_0——is the ambient temperature;
K_T——overall coefficient of heat transfer;

According to experiment experience, the category of overall coefficient of heat transfer is between 6 and 20. Overall coefficient of heat transfer can be defined as 8 or 10 W/(m^2·K). The paper is organized as follows: The GIS model description is illustrated in Section 2. The GIS meshed model is presented in Section 3. GIS simulation studies and temprature test is explained in section 4. conclusion is concluded hereinafter.

2. Model description

2.1. Thermoelectric coupling simulation of GIS

The gas insulated switchgear (GIS) is composed of isolators that open/close and cut off circuits of current, disconnectors that electrically isolate circuits and open voltage, and other components. GIS is the name for a unit that houses these components and circuits in a single gas tank with a compact footprint (Tschentscher and Franck, 2018; Xue et al., 2018). Grounding devices that prevent electrical shock and lightning arresters that prevent dielectric breakdowns from lightning strikes are also included to enhance safety. Gas insulated switchgear plays a vital role acting as a huge switch to operate and protect substations. A geometry model of 252 kV is drawn in Fig. 2.

2.1.1. Circuit breaker and current transformer

The circuit breaker is usually in a separate enclosure because of the higher gas pressure requirement for its arc distinguishing capability. The circuit breaker module may be horizontal or vertical oriented and is the base module of a bay. Other modules are connected to it as shown in Fig. 3. The compartment usually has a higher operational pressure (0.7 MPa to 0.8 MPa) than the other modules (0.4 MPa to 0.6 MPa) because of the need to

distinguish the switching arc for interruption of rated currents (2000A to 5000 A) or in case of short circuits (25 kA to 80 kA). The circuit breaker housing is used as the basis of the bay to which disconnectors, ground switches, and bus bars are connected. Since one of the main purposes of a circuit breaker is to automatically and rapidly de-energize faulted transmission lines, transformer banks and buses. An opening operation is initiated by protective relays, which are generally installed remotely in a relay and control room.

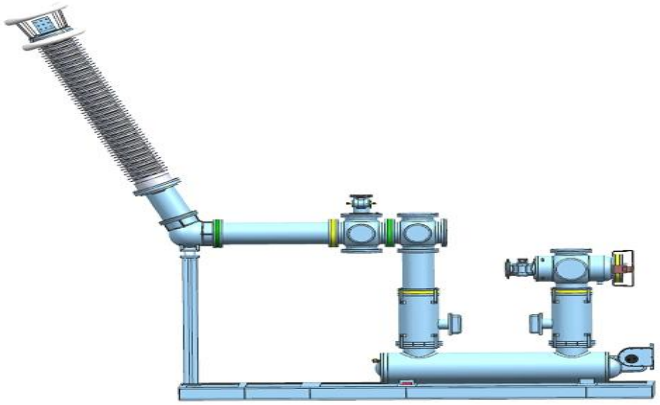

Fig. 2. Geometry model of 252 kV GIS.

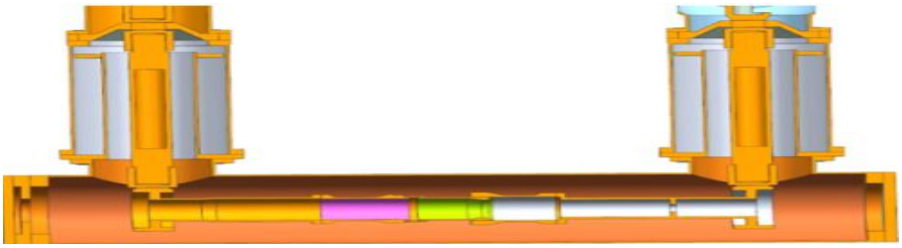

Fig. 3. GIS circuit breaker and current transformer.

This operation may include automatically reclosing of the circuit breaker one or more times. The opening or closing of a circuit breaker can also be initiated by human intervention from several locations, including manually from the circuit breaker mechanism cabinet, electrically from the local control cabinet, from the relay and control panels remote from the circuit breaker, or from supervisory controls remote from the substation. A circuit breaker, generally, is not prevented (interlocked) from opening and/or closing by the position of either a disconnect switch or a grounding switch. However, a circuit breaker is prevented from operating or is automatically required to operate by parameters that affect its successful function, such as low interrupting and insulating gas density, low mechanism pressure, pole disagreement tripping (in case of circuit breakers with independent pole operation), or monitoring of the proper position of the circuit breaker before initiating an operation. As an example, a circuit breaker must be in the fully closed position before an open operation can be initiated and, conversely, a circuit breaker must be in the fully open position before a close operation can be initiated. The indication of the position of the circuit breaker can be monitored at the circuit breaker mechanism cabinet via mechanically operated semaphores, at the local control cabinet, at the relay and control panels remote from the circuit breaker, or from supervisory controls remote from the substation with positions indicating red and green lights or semaphores.

In the current transformer the primary is connected to the power line in the series, so the primary is nothing it is only the current which flow through the power line and it does not depend on the load. Gas compartment reduces the access of moisture and to suppress gas tight bushing for secondary connections. Current transformer is generally located in the circuit breaker bushing turrets, however specific designs involving direct cable or transformer connections may require standalone CTs. As in the case of AIS standard current injection and ratio tests can be performed. However, to access the main bus as stated earlier, ground switches will need to be isolated and the test currents or voltages injected thru the ground switch onto the bus. These tests are conducted with the main bus denergized and isolated from any operational portions of the remaining GIS switchyard. It is also important to remember when the tests are completed before the bus or equipment is energized, the CTs must be connected or shorted, otherwise equipment damage may result.

2.1.2. Fast acting earthing switch's

An Earthing switch is used for the protection and it has the slowest operation. These switches are to be vertically broken switches. The earthing arm interlocked with main isolator moving contact. When the main contact of isolator will be close, then it will be open. Similarly the main contact of isolator will be open when earthing arms will be inclose position. It operated only when it is a High voltage system is not energized. Fast acting earthing switches have the additional capability of closing an energized conductor, creating a short circuit without receiving significant damage to the switch or the enclosure. Fast acting earthing switches are also used to ground various active elements of the substation, such as transmission lines, transformer banks, and main buses. In some GIS facilities high speed ground switches are used to initiate protective relay functions. They are typically not installedin ground circuit breakers or voltage transformers. Fig. 4 is depecting the overview of GIS fast earthing switch.

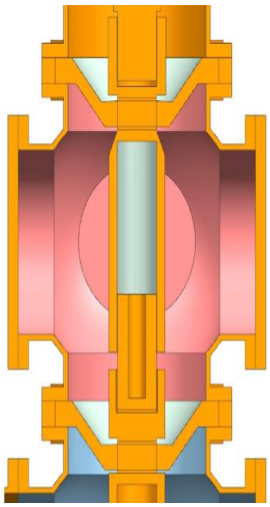

Fig. 4. GIS fast earthing switch's.

Fast acting earthing switches are also designed and tested to interrupt electrostatically induced capacitive currents and electromagnetically induced inductive currents occurring in de-energized transmission lines in parallel and close proximity to energized transmission lines. They can also remove DC trapped charges on a transmission line. High speed (fault-initiating) grounding switches typically have motor operating mechanisms with spring assists for rapid opening and closing of the switchblade. They typically use the same methods for determining the switch position as disconnect switches.

2.1.3. Disconnectors

Specially developed "load-break disconnectors," which cannot interrupt a short-circuit current, only the load current of the switchgear, can fulfill the functions of the disconnector. These load-break disconnector switches are used if a circuit breaker is available in the network to clear short-circuit currents.

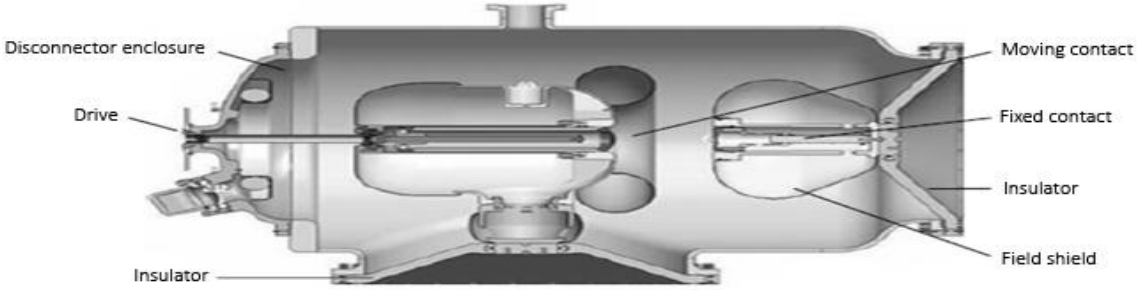

Fig. 5. Cross section of a GIS disconnector.

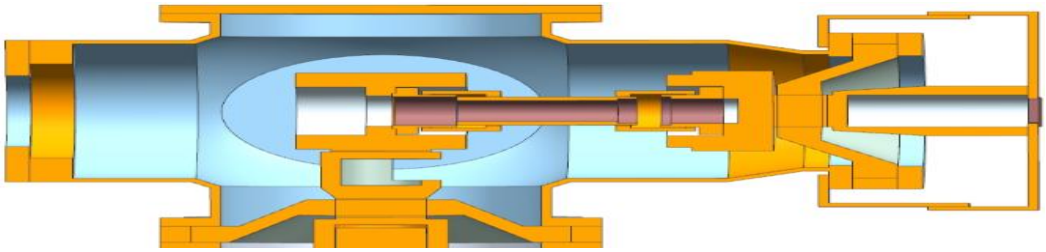

Fig. 6. GIS disconnetors.

For normal load current interruption the load-break disconnect switch can be operated. Disconnector switches in a GIS are installed for the same purpose as those in an air insulated substation (AIS). They are used to isolate various components of the substation, such as circuit breakers, transmission lines, transformer banks, buses and voltage transformers. They generally do not have significant interrupting capability except for small quantities of charging current associated with short pieces of bus. These charging currents are in the range of 0.5 A to 2.0 A. Fig. 5 and Fig. 6 are depicting the cross section of GIS connector and disconnector, respectively.

2.1.4. Gas insulated line (GIL)

GIL consists of a central aluminum conductor with a typical electrical cross section of up to 5,300 mm^2. The conductor rests on cast resin insulators, which center it within the outer enclosure. This enclosure is formed by a sturdy aluminum tube, which provides a solid mechanical and electrical containment for the system. To meet up-to-date environmental and technical aspects, GIL is filled with an insulating gas mixture of main nitrogen (usually 80% and a smaller percentage of SF_6 (20%). The GIL overview is presented in Fig. 7.

2.1.5. L-Shape connector

An L-Shaped connector, which can waterproof simply and connect an L-Shape terminal to an electric shield wire in miniaturized size so as to insulate and electromagnetic shield the L-Shaped terminal, includes an L-Shaped dividable insulation inner housing receiving an L-Shaped terminal joined to the electric shield wire; an electric conductive shield shell covering a terminal receiving portion of the inner housing; an outer housing covering the shield shell; an electric conductive housing receiving a wire lead-out portion of the inner housing. Fig. 8 is showing the L-Shaped connector's overview.

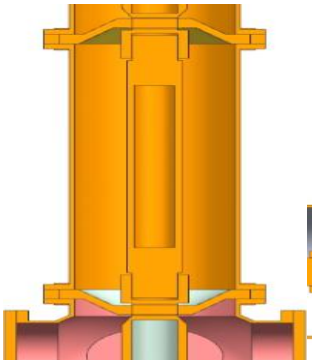

Fig. 7. Gas insulated line (GIL).

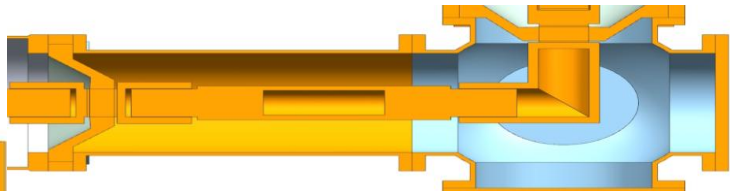

Fig. 8. L-Shape connector.

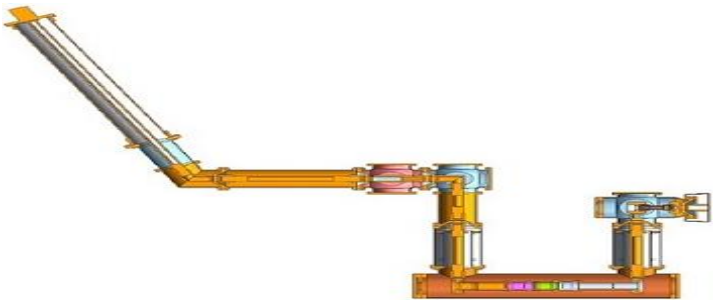

Fig. 9. Simplified model of GIS.

Joining a flange of the shield shell and a flange of the outer housing to a flange of the electric conductive housing by screwing, and connecting a shield portion of the electric shield wire through a shield terminal to the shield shell; and a shield packing waterproofing between the flange of the shield shell and the flange of the electric conductive shell. In Fig. 9, the simlified model of GIS describe the main component of Gas Insulated switchgear. Currnet transformer, Circuit breaker, compound bushing, bus bar compartment, L-Shape connector, disconnectors and earthing switches.

3. GIS meshed model

3.1. Contact resistance

The modern high voltage SF_6 circuit breakers have two parallel contact sets. The main contacts are low resistance contacts, which are silver plated, whereas arcing contacts are of tungsten-copper, which helps in initiating arc quenching and current interruption. Measurement of the static contact resistance with the breaker in closed position gives the resistance of main contacts only because the arcing contacts are bypassed. Static contact resistance is measured by injecting a DC-current through the breaker and measuring the milli-voltage drop. A four wire measurement method is used (Yanabu et al., 2002; Küchler, 2018). The breaker must be in the closed position. If low resistance readings are obtained when testing the breaker contact resistance using a low current, then it is recommended to re-test the contacts at a higher current. A higher current will have the ability to overcome connection issues and oxidation on terminals, where a lower current may produce higher readings under these conditions. The Fig. 10 and 11 are depicting the meshed model of GIS and 3D tetrahedron mesh generation of GIL-CB.

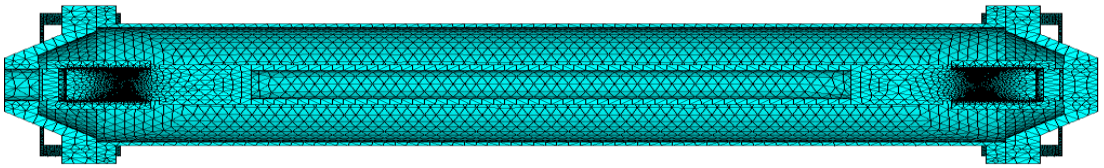

Fig. 10. Meshed model of GIL.

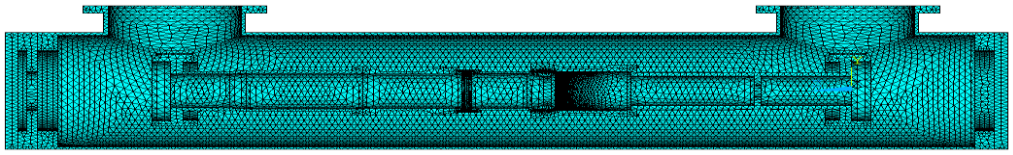

Fig. 11. Meshed model of CB.

The limitation of static contact resistance measurement is that, it ignores the information about the arcing contact condition. Erosion of arcing contact, contact misalignment, damage to driving mechanism cannot be detected from static contact resistance measurement. Dynamic contact resistance measurement for circuit breakers was introduced in 1992 (Bhole and Gandhara, 2016).

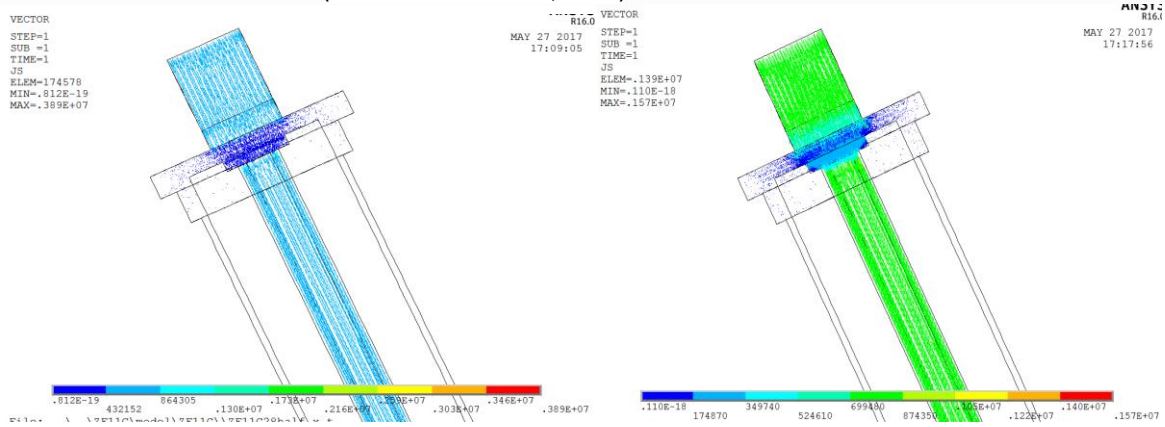

(a) (b)

Fig. 12. Current density of compound bushing upper side (thermal source calculation).

The current density distribution of compound bushing upper side is shown in Fig. 12. The part (a) ignores the contact resistance and current density of part (a) is lower than part (b). Part (b) care about the contact resistance and current density of part (b) is higher than part (a). While in Fig. 13, the current density distribution of compound bushing lower side is shown. The part (a) do not consider the contact resistance and current density of part (a) is lower than part (b). The part (b) consider the contact resistance.

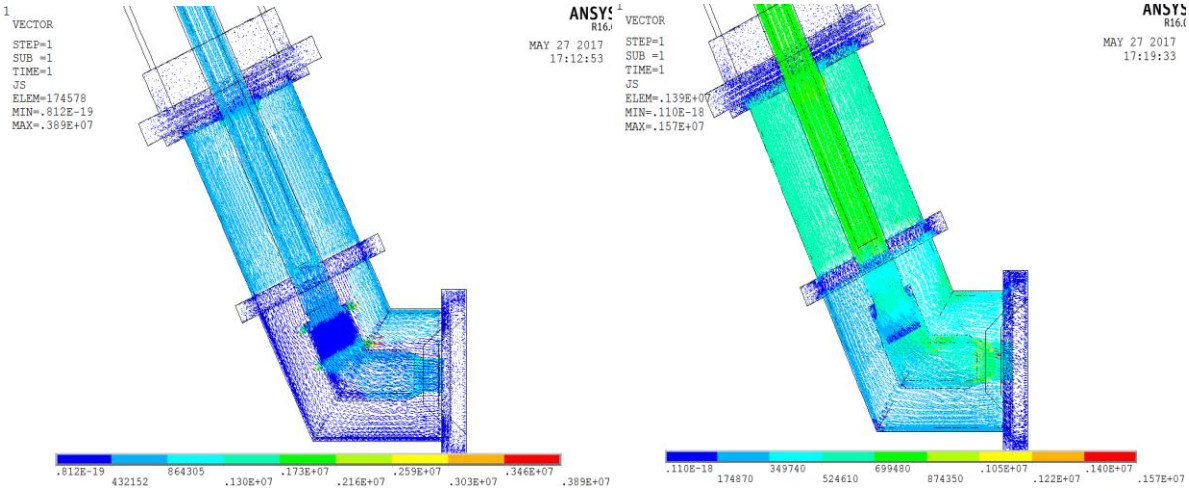

(a) (b)

Fig. 13. Current density of compound bushing lower side.

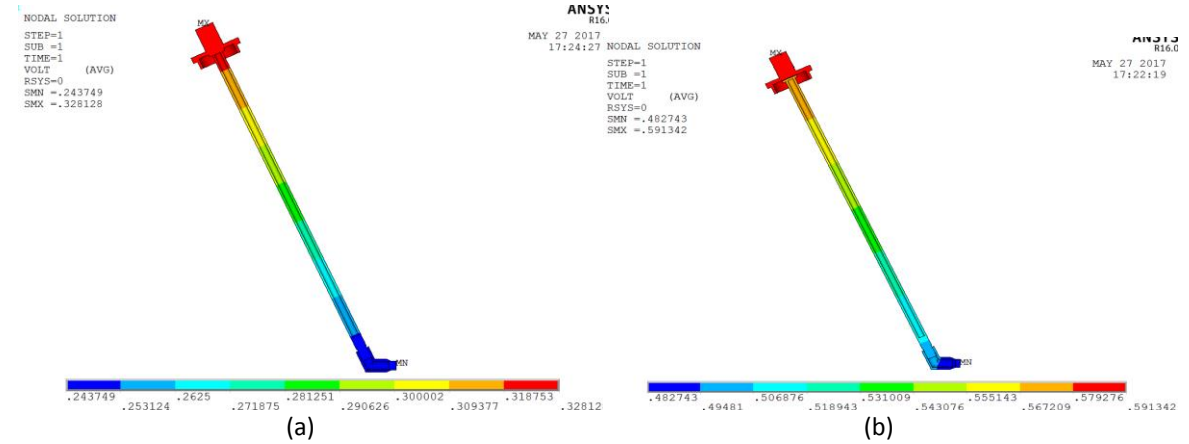

(a) (b)

Fig. 14. Electric potential density of compound bushing.

The potential difference of compound bushing part (a) is 0.084379 V and the loop resistance of compound bushing is 21 μΩ. Potential difference of compound bushing part (b) is 0.108599 V. The loop resistance of compound bushing is 27 μΩ. In compound bushing, there are three contacts and each contact resistance is 2 μΩ. So, the total contact resistance is 6 μΩ.

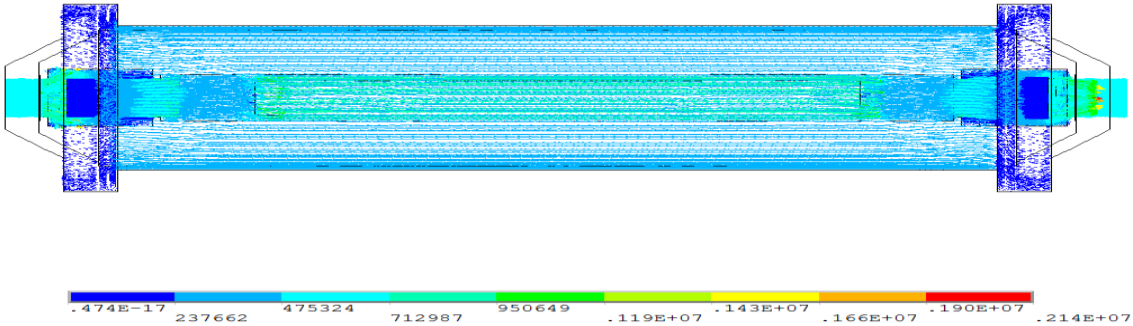

Fig. 15. Current density distribution of busbar compartment.

Fig. 15 and 16 depcits the bus bar compartment contact resistance is being considered. Both current density of contacts area are bigger than shell and bus.

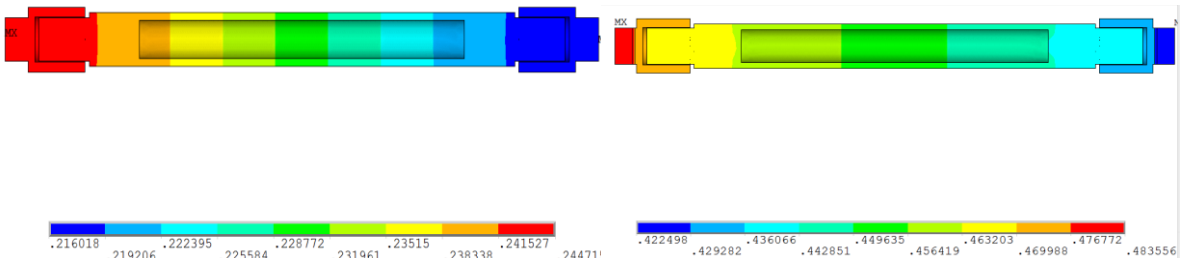

(a) (b)

Fig. 16. Electric potential density of busbar compartment.

The potential difference of busbar compartment part (a) is 0.028697 V and the loop resistance of busbar compartment is 7 μΩ. Potential difference of compound bushing part (b) is 0.061058 V and the loop resistance of busbar compartment is 15 μΩ.

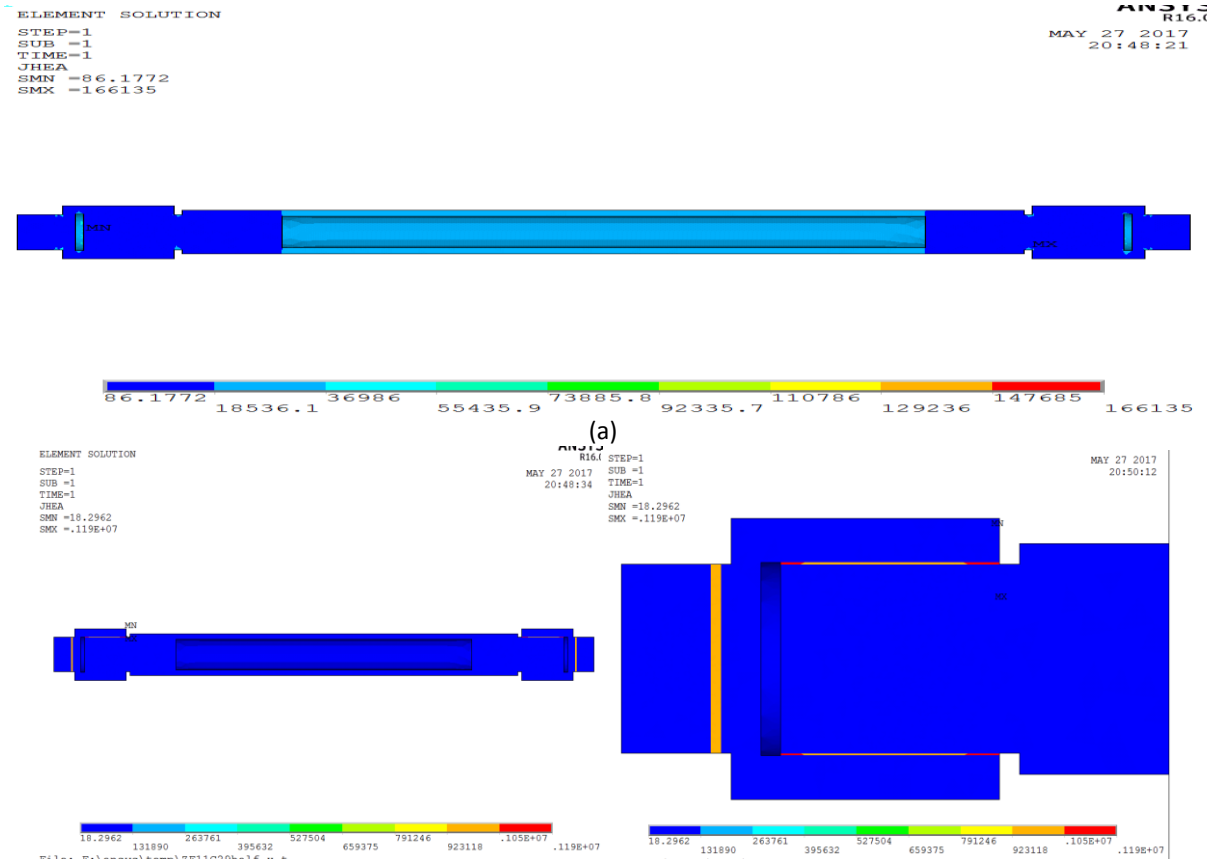

(a) (b) (c)

Fig. 17. Joule heat of busbar compartment.

Fig. 17 shows the joule heat of busbar compartment. In part (a) contact resistance is not considered and in part (a) the bus area is bigger than other areas and also produce the joule heat higher than other areas. In parts (b) and (c) contact resistance is considered. In part (c) the area of fixed contact and spring contact is bigger than other areas and they produce higher joule heat as compared to other areas.

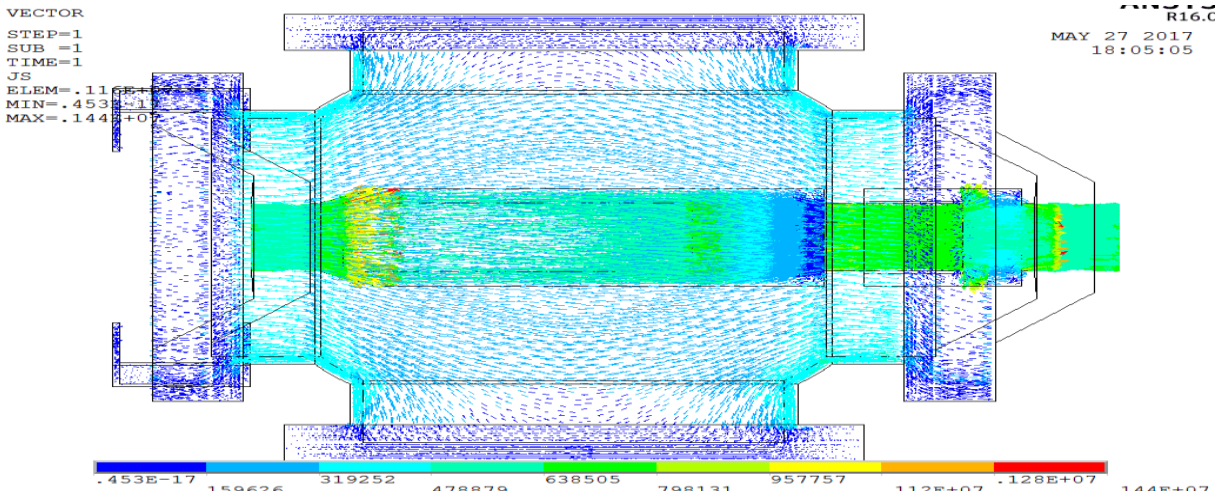

Fig. 18. Current density distribution of fast earting switch (FES).

In Fig. 18, the fast earthing switch is considers contact resistance. Both current density of contact areas are bigger than shell and bus. While the Fig. 19 shows the current density distribution of L-shape connector. The part (a) care about contact resistance. The part (b) does not care about the contact resistance. In Fig. 20, the current transformer considered the contact resistance. Both current density of contact areas are bigger than shell and bus.

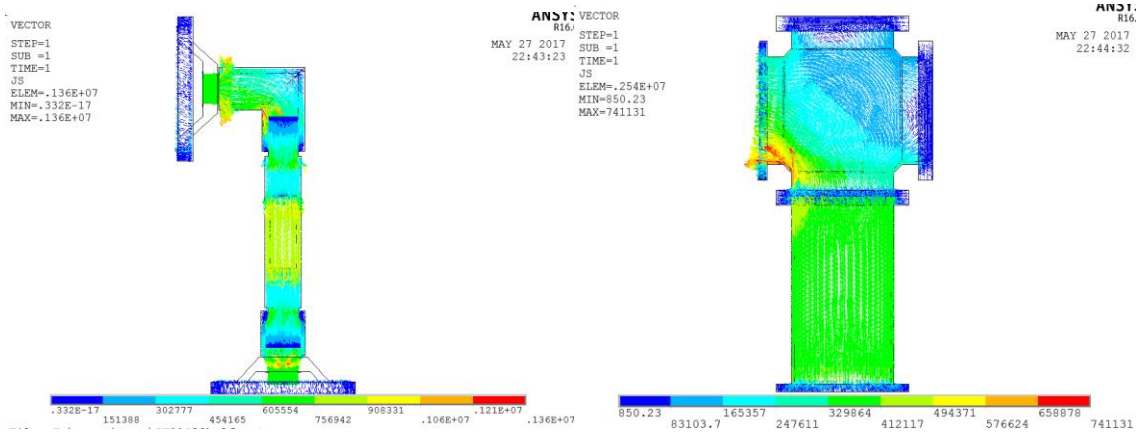

(a) inside conductor (b) shell

Fig. 19. Current density distribution of L-Shape connector.

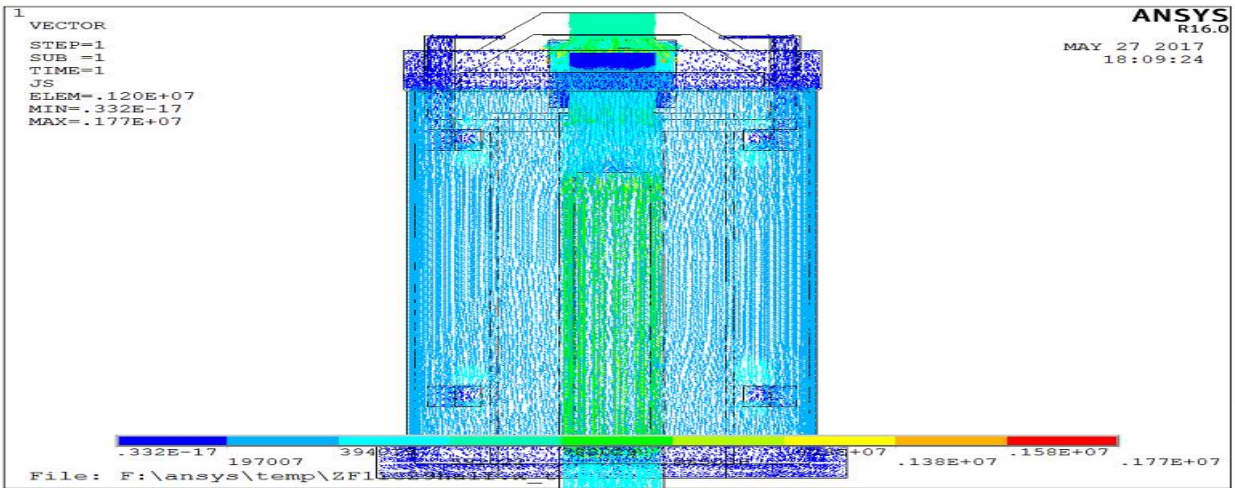

Fig. 20. Current density distribution of current transformer.

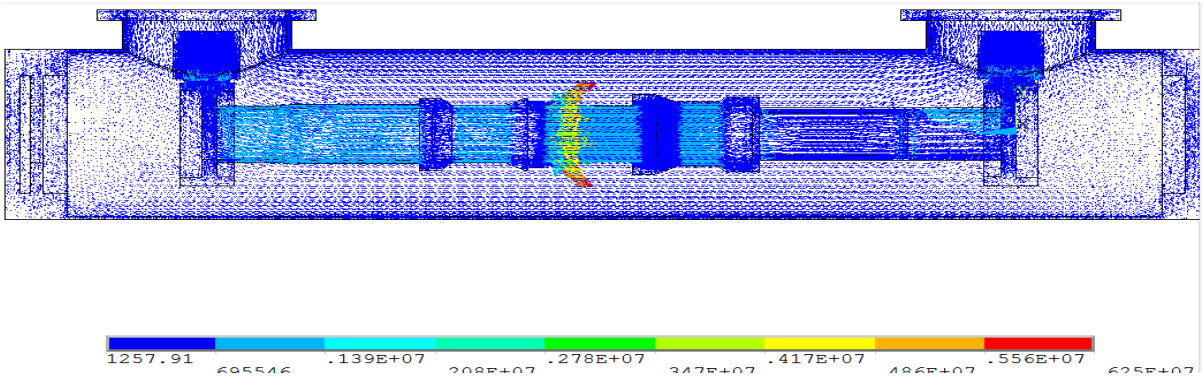

Fig. 21. Currentdensity distribution of circuit breaker.

In Fig. 21, thecircuit breaker is considered the contact resistance. Both current density of contacts area are bigger than shell.

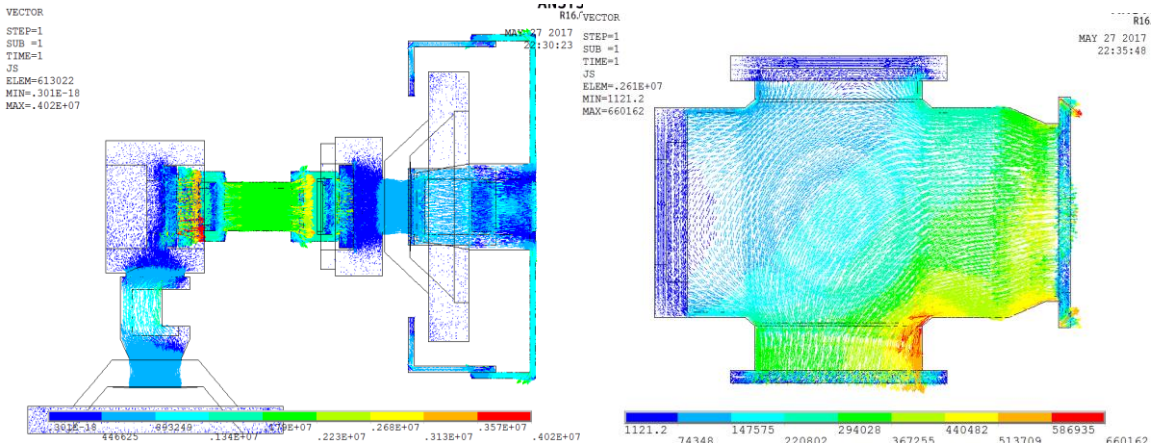

(a) (b)

Fig. 22. Current density distribution of disconnector.

Fig. 22 shows the current density distribution of disconnector. Part (a) consider contact resistance. Part (b) doesn't consider the contact resistance.

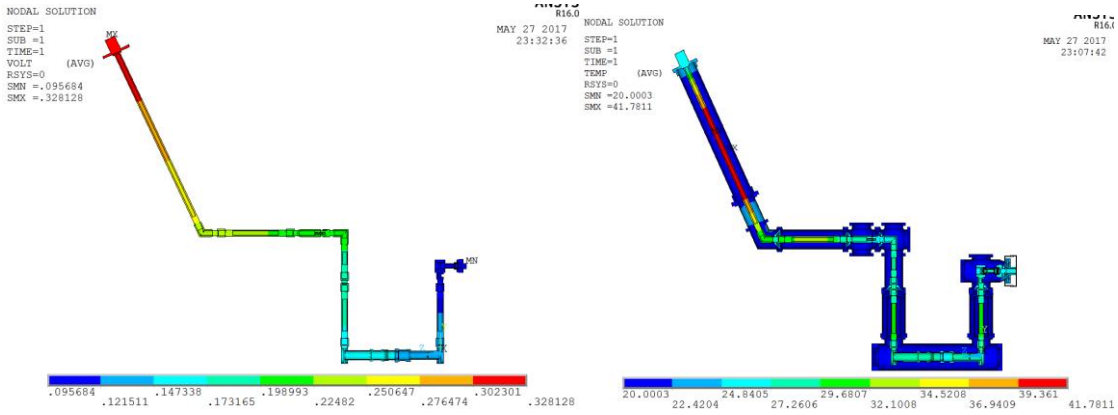

(a) (b)

Fig. 23. GIS DC thermoelectric coupling (during current flow outside shell).

When current flow in outside of the shell depicted in Fig. 23 part (a) then the contact resistance is ignored and its loop resistance measured 58 μΩ. In part (b), maximum temperature rise is measured 21.78 °C.

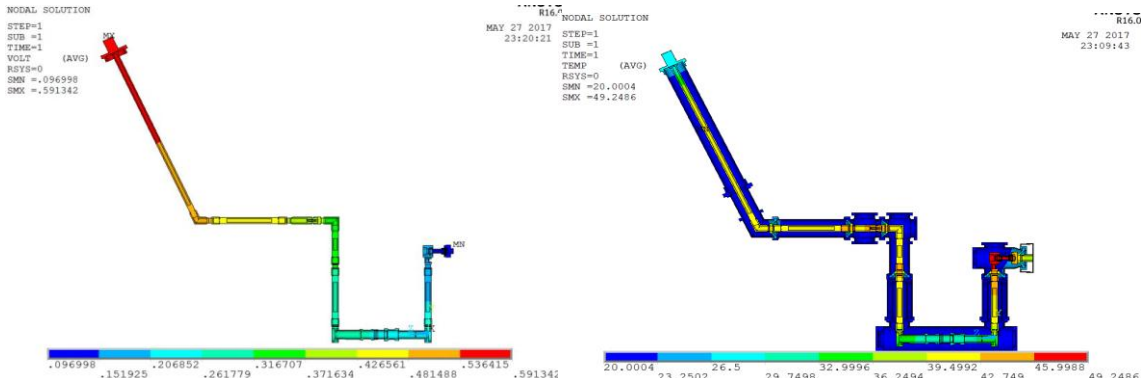

Fig. 24. Current flow outside shell and contact resistance (considered).

When current flows in the outer shell of the diagram part (a) then the contact resistance will be considered the loop resistance is 124 μΩ. In part (b) GIS max temperature-rise is 30 °C. Fig. 24 depicted the current flow with considering the contact resistance of outside of shell.

4. GIS simulation studies and temperature test

4.1. Simulation studies

Simulation of meshed equipments of GIS and temperature is tested in this section. The current density distribution and power loss of busbar compartment are depicted in Fig. 25.

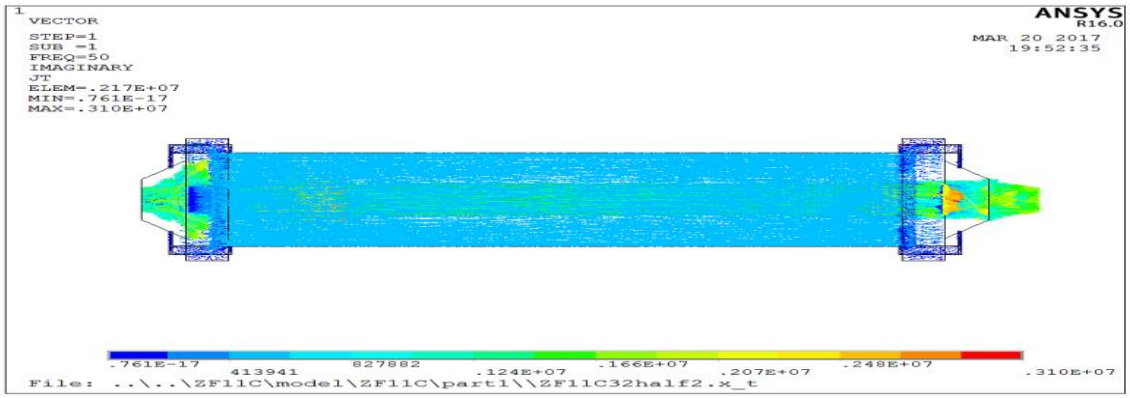

Fig. 25. Gas insulated line (power losses).

Table 1
Busbar compartment power losses.

Part name	Power loss	Volume	Power density
Spring contact base (left)	25	6.0E-04	42759
Busbar	75	3.6E-03	20632
Spring contact base (right)	25	6.0E-04	42759
Shell	28	7.6E-03	3711
Conductor in basin-type insulator	36	1.4E-04	251996
Outside lane of basin-type insulator	0.7	8.8E-04	768

In Table 1, the power density of conductor in basin type insulator is bigger than other parts because in “conductor in basin type insulator” includes the power loss which contact resistance generated. The current density of two contants bigger than other parts which is depicted in Fig. 26.

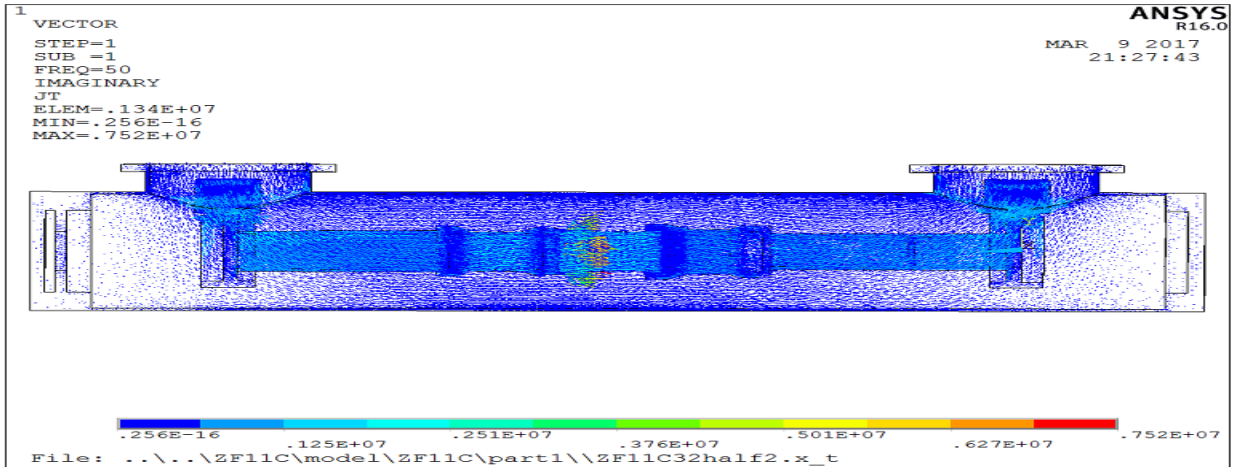

Fig. 26. Circuit breaker (power losses).

Table 2
Circuit breaker power losses.

Part name	Power loss	Volume	Power density
Contact base	35	2.7E-03	13702
Fixed contact base	12	1.0E-03	12025
Peel contact finger	33	1.4E-04	241168
Moving contact	10	4.1E-04	25259
Wristband contact finger	16	2.2E-05	730705
Gas compress vat	11	1.3E-03	8490
Contact base	42	3.3E-03	12358
Shell	38	2.3E-02	1623
Left inside cover	0.05	2.9E-03	16
Left outside cover	0.02	2.7E-03	6
Right cover	0.05	3.1E-03	17

In Table 2, the power density of wrisband contact finger is bigger than other parts because in “conductor in basin type insulator” includes the power loss which contact resistance generated.

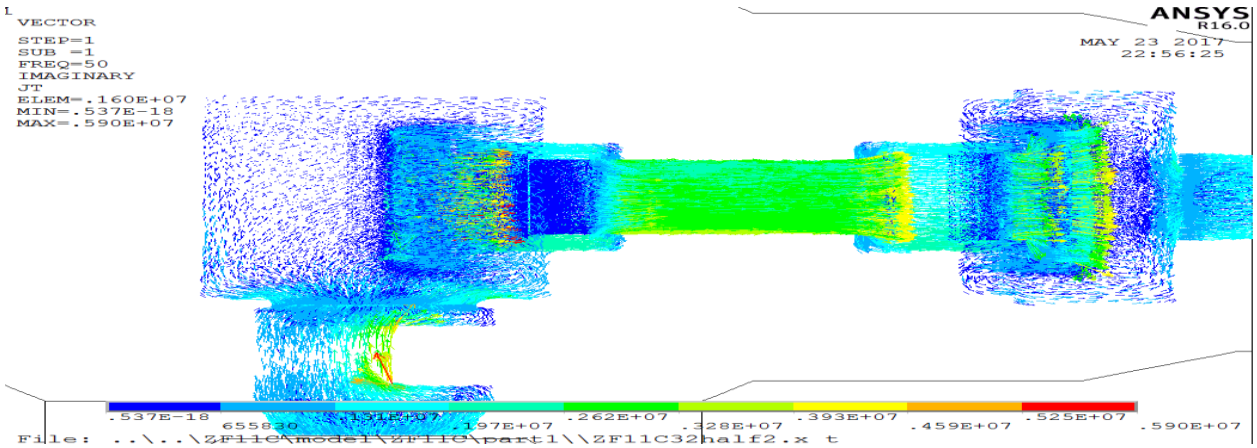

Fig. 27. Disconnector (DES power losses).

In Table 3, the power density of thin layer is bigger than other parts and its power density is 1257520. While, the Table 4 is depicting the power density of “conductor in basin type insulator” is bigger than other parts because “conductor in basin type insulator” includes the power loss which contact resistance generated. “Conductor in basin type insulator” maximum power density is 252071.

Table 3
Disconnector power loesses.

Part name	Power loss	Volume	Power density
Conductor in basin-type insulator	19	1.4E-04	138614
Outside lane of basin-type insulator	0.8	8.8E-04	884
Thin layer	12	9.5E-06	1257520
Contact base	27	4.3E-04	62218
Moving contact base	15	1.9E-03	7788
Contact base	2	1.2E-04	18477
Peel contact finger (left)	37	1.3E-04	269307
Moving contact	9	1.8E-04	54412
Peel contact finger (right)	37	1.3E-04	268337
Contact base	2	1.8E-04	12661
Fixed contact base	14	1.3E-03	10553
Thin layer	12	1.5E-05	754512
Conductor in basin-type insulator	20	1.4E-04	138931
Outside lane of basin-type insulator	2	8.8E-04	2864
Shell	17	9.1E-03	1850
Up cover	0.1	1.8E-03	76
Left cover	0.03	1.5E-03	20

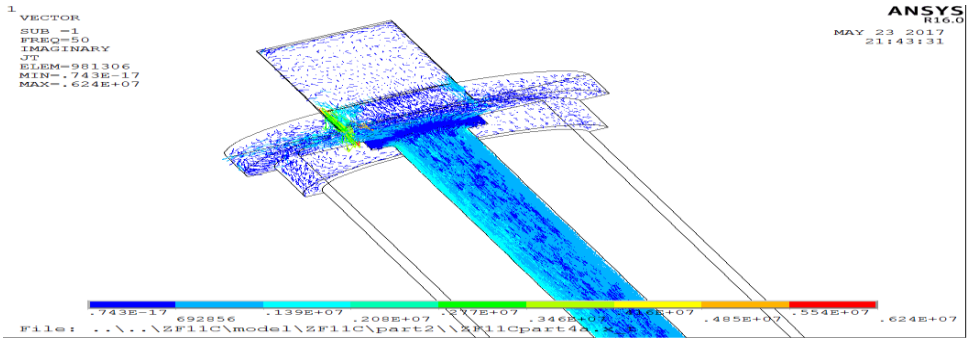

Fig. 28. Compound bushing (power losses).

Table 4
Compound bushing power loesses.

Part name	Power loss	Volume	Power density
Incoming terminal	51	4.1E-03	12172
Up flange	8	2.0E-03	4194
Busbar	192	8.4E-03	22784
Down flange	19	2.9E-03	6706
Down flange plate	25	3.4E-03	7382
Medium shell	34	3.1E-03	11178
L-Type conductor	16	1.2E-03	12970
Conductor in basin-type insulator	36	1.4E-04	252071
Outside lane of basin-type insulator	0.7	8.8E-04	881
L-Type shell	14	4.3E-03	3306

4.2. GIS temperature-rise test

According to temperature-rise test data, GIS maximum temperature-rise is 57 °C. To prove at what maximum continuous current the GIS can be operated, a temperature rise test is performed. Thermocouples are placed at various locations such as conductors, connections, contacts, and insulators to measure the temperature rise at a defined continuous current the GIS are designed for. Other than this discrete measure method, by using

thermocouples additional thermo graphic measures can be used to support the analysis of the arrangement related to the temperature rise, especially during development tests. The test setup of the GIS including the circuit breaker, disconnect switch and bus bar is shown in Fig. 27 and 28. Figure show the test setup of the GIS enclosure.

Fig. 29. GIS temperature rise-test model.

There are 4 pieces of aluminum bus bar at incoming ends together, each length is 2 m and the dimension is 15 mm × 150 mm, there are 2 pieces of separately copper bus bar at outgoing ends, each length is 2 m and the dimension is 10 mm × 120 mm. The GIS temperature rise-test parameters are acknowledged in Table 5, while the resistance of the main circuit in temperature rise-test is tabled in Table 6. The temperature rise-test model and circuit diagram is presented in Fig. 29 and 30.

Table 5
GIS temperature rise-test parameters.

Contents	Values (unit)
Current frequency	50 Hz
Ambient wind speed	<0.5 m/s
SF_6 gas pressure of CB gas compartment	0.50 MPa
SF_6 gas pressure of other gas compartment	0.43 MPa
Ambient temperature	23.4 °C
Ambient humidity	57.9 %

Table 6
Resistance of the main circuit in temperature-rise tests.

	Before temperature-rise tests	After temperature-rise tests
Test result (μ)	118	123
Ambient temperature	24.0 °C	22.6 °C

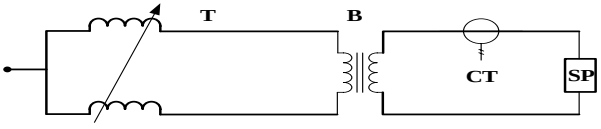

Fig. 30. Test circuit diagram.

T-Voltage adjuster; B-Transformer; CT-Current transformer; SP-Test object.

4.3. Simulation results

ANSYS software platform is utilized for modeling of GIS parameters. The current, initial temperature, ambient temperature, external heat transfers and coefficient SF_6 gas pressure of CB gas compartment are modeled. For the different conditions the amount of current is different, but the other parameters are measured same because the current occurs the change in temperature and the ambient temperature is measured 23.4°C. The GIS temperature field simulation result is shown in Fig. 31. The maximum temperature value of GIS is 352 and it is located in current transformer. The minimum temperature value is 317.

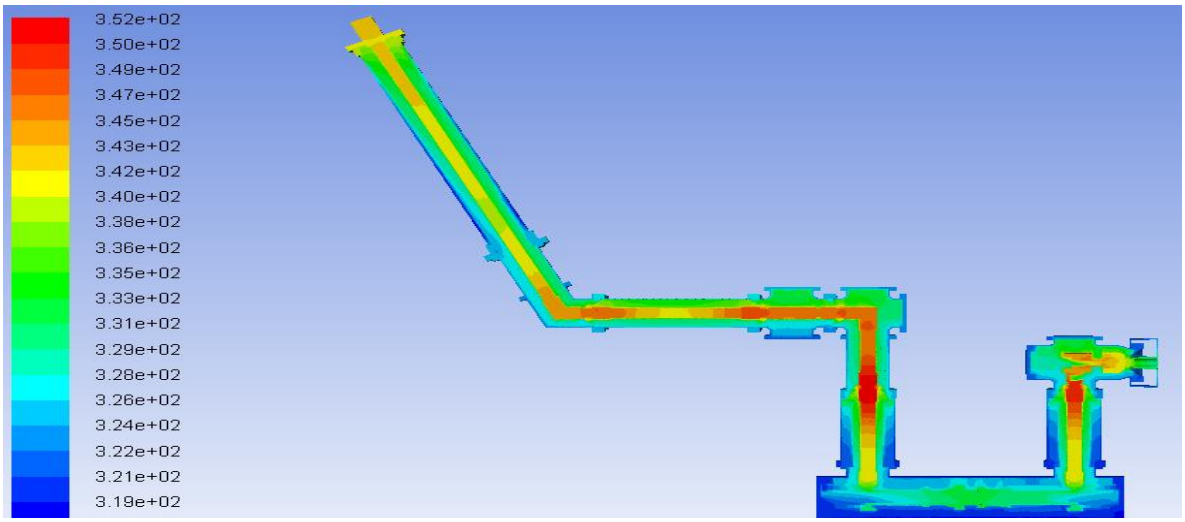

Fig. 31. GIS temperature field simulation results.

Table 7
Circuit breaker temperature results.

CB	Test data	Simulation data	Difference data
Spring contact (left)	42	45	-3
Contact base	28.5	31	-2.5
Fixed contact base	31	35	-4
Peel contact (left)	37	38	-1
Moving contact	35	38	-3
Spring contact (right)	38	40	-2
Contact base	32	36	-4
Spring contact (right)	41	45	-4
Shell	23	25	-3

In Table 7, the maximum simulation value of spring contact (left and right) is 45. The minimum simulation value of the shell is 25. Test data and simulation data is less than 4 k from difference value. In Table 8, the maximum simulation value of spring contact (down) is 56. The minimum simulation value of the contact base is 50. Test data and simulation data is less than 5 k from difference value.

Table 8
L-Shape contact tube temperature results.

L-Shape contact tube	Test data	Simulation data	Difference data
Spring contact (down)	57	56	1
Bus (down)	50.5	53	-2.5
Bus (up)	49	52	-3
Contact base	45	50	-5

Table 9
FES contact tube temperature results.

FES	Test data	Simulation data	Difference data
Contact base	47	51	-4
Moving contact	46	50	-4
Bus	46	50	-4
Gas	27	31	-4

The Table 9 is depicting the maximum simulation value of contact base is 51. The minimum simulation value of the gas is 31. Test data and simulation data is less than 4 k from difference value.

Table 10
DES contact tube temperature results.

DES	Test data	Simulation data	Difference data
Contact base	47	51	-4
Peel contact finger (left)	48	50	-2
Moving contact	47	50	-3
Peel contact finger (right)	45.5	49	-3.3
Fixed contact base	39	44	-5
Experimental joint	33	37	-4
Connecting plate 1	27	30	-3
Connecting plate 1	20.5	25	-4.4
Shell	22	27	-5

The maximum simulation value of contact base is 51 in Table 10. The minimum simulation value of the connecting plate 1 is 25. Test data and simulation data is less than 5 k from difference value.

Table 11
Gas insulated line (GIL) temperature results.

GIL	Test data	Simulation data	Difference data
Contact base (right)	52	50	2
Bus	53.5	48	5.5
Contact base (left)	51	50	1

In Table 11, the maximum simulation value of contact base (left, right) is 50. The minimum simulation value of the bus is 48. Test data and simulation data is less than 5 k from difference value. While, in Table 12, the maximum simulation value of spring contact is 50. The minimum simulation value of the L-Shape conductor is 26. Test data and simulation data is less than 5 k from difference value.

Table 12
Compound bushing temperature results.

Compound bushing	Test data	Simulation data	Difference data
L-Shape bus	43	48	-5
Spring contact	51	50	1
Bus	47	47	0
Incoming terminal	46	48	-2
L-Shape shell	21	26	-5
Gas	33	35	-2

A comprehensive exploration of GIS equipment simulation, temperature test and power losses of GIS components have been made. Analysis and simulation results show the criteria for detecting fault direction, which works perfectly under various fault conditions and satisfies the criteria requirement. From GIS components temperature results, the maximum simulation values are 45, 56, 51, 51, 50 and 50. The minimum simulation value are 25, 50, 31, 25, 48 and 26. Test data and simulation data is less than 5 k from difference value.

5. Conclusion

The installation of SF_6 switchgear brought advantages in performance, size, weight, overall cost and reliability under multi operating conditions. According to the structure of GIS, the model is being built and simulated for temperature rise-test. The simulated and experimental results are compared. The temperature rises at the

conductors contact part which is closely related to the increasing loop resistance, especially the contact resistance. The temperature rises with the loop resistance. The highest temperature area generally locates around the contact part. Temperature field is designed and its availability, reliability was verified by comparing the simulation results with the test data. Then different contact conditions are fixed and the corresponding temperature rising characteristics obtained. According to the simulation and experiment study, by measuring the loop resistance, condition estimate of abnormal contacts can be accomplished. On the ground, a reasonable maintenance strategy can be drawn up and loop resistance measured 124 μΩ. Maximum temperature of GIS measured 352 k. Temperature rising value is 56 k, which is located between current transformer and L-Shape conductor, whereas discrepancy is less than 5 k. Simulation studies carried out to incorporate the protection schemes which are comparatively effective in terms of reliability and economic aspect.

References

Arumugam, S., Haba, Y., Koerner, G., Uhrlandt, D., Paschen, M., 2018. Understanding partial discharges in low-power relay and silicone cable modified to suit high-voltage requirement of deep sea electrical system. International Transactions on Electrical Energy Systems.

Bhole, A.A., Gandhara, W.Z., 2016. An overview of dynamic contact resistance measurement of HV circuit breakers. J. Inst. Eng. India Ser. B., 97(2), 219-226. https://doi.org/10.1007/s40031-014-0164-2

Chmielewski, T., Oramus, P., Szewczyk, M., Kuczek, T., Piasecki, W., 2017. Circuit breaker models for simulations of short-circuit current breaking and slow-front overvoltages in HV systems. Elec. Power Syst. Res., 143, 174-181.

Koch, H., 2014. Gas Insulated Substations. John Wiley and Sons.

Küchler, A., 2018. Electric stresses. High Voltage Engineering. Springer Berlin Heidelberg, 5-140.

Küchler, A., 2018. Testing, measuring and diagnosis. High Voltage Engineering. Springer Berlin Heidelberg, 355-496.

Kuwahara, H., Tanabe, T., Sasamoto, S., Nitta, T., 1982. Experiences in maintaining the quality of gas insulated equipment in the field and their feedback to the design and the manufacturing processes. Gaseous Dielectrics III., 475-483.

Lee, B.H., Jeon, S.D., Lee, J.H., Kim, D.W., 2011. Development of GIS fault section detection system. Electric Power Equipment-Switching Technology (ICEPE-ST), IEEE 1st International Conference.

Li, X., Wang, B.J., Wang, X.Q., 2012. Research progress on temperature monitoring of GIS bus. High Voltage Apparatus, 11, 027.

Li, Y., Shang, Y., Zhang, L., Shi, R., Shi, W., 2012. Analysis of very fast transient over voltages (VFTO) from onsite measurements on 800 kV GIS. IEEE Transactions on Dielectrics and Electrical Insulation, 19(6).

Misrikhanov, M.S., Mozgalev, K.V., Shuntov, A.V., 2003. Reliability of gas insulated substations and switchgears with traditional insulation. Power Technology and Engineering (Formerly Hydrotechnical Construction), 37(6), 377-383.

Nazir, M.S., Wu, Q., Li, M., Zhang, L., 2017. Symmetrical short circuit parameter differences of double fed induction generator and synchronous generator based wind turbine. Indonesian J. Electr. Eng. Comput. Sci., 6(2), 268-277.

Okubo, H., Yanabu, S., 2002. Feasibility study on application of high voltage and high power vacuum circuit breaker. 20th International Symposium on Discharges and Electrical Insulation in Vacuum, IEEE.

PD IEC-TS 62478, 2016. High voltage test techniques-measurement of partial discharges by electromagnetic and acoustic methods. BSI, London, UK.

Qi, B., Gao, C., Li, C., Zhao, L., Sun, X., 2015. Effect of surface charge accumulation on flashover voltage of GIS insulator in SF6 under DC and AC voltages. Electrical Insulation and Dielectric Phenomena (CEIDP), IEEE Conference Publication.

Riechert, U., Holaus, W., 2012. Ultra high-voltage gas-insulated switchgear - a technology milestone. International Transactions on Electrical Energy Systems, 22(1), 60-82.

Schueller, M., Straumann, U., Franck, C.M., 2014. Role of ion sources for spacer charging in SF_6 gas insulated HVDC systems. IEEE Transactions on Dielectrics and Electrical Insulation, 21(1), 352-359.

Shioiri, T., Honma, M., Miyagawa, M., Kaneko, E., Ohshima, I., 1999. Insulation characteristics of vacuum interrupter for a new 72/84 kV C-GIS. IEEE Transactions on Dielectrics and Electrical Insulation, 6(4), 486-490.

Switchgear, High-voltage, 2001. Controlgear-part 100: High-voltage alternating-current circuit-breakers. Edition 1, 62271-100.

Takahashi, T., Okamoto, T., Ohki, Y., Shibata, K., 2005. Breakdown strength at the interface between epoxy resin and silicone rubber-a basic study for the development of all solid insulation. IEEE Transactions on Dielectrics and Electrical Insulation, 12(4), 719-724.

Tschentscher, M., Franck, C.M., 2018. A critical reexamination on conduction processes in gas-insulated HVDC devices at low electric fields. IEEE Transactions on Dielectrics and Electrical Insulation, GI-TL.

Ueta, G., Tsuboi, T., Takami, J., Okabe, S., Ametani, A., 2014. Insulation characteristics of gas insulated switchgear under lightning impulse and AC superimposed voltage. IEEE Transactions on Dielectrics and Electrical Insulation, 21(3), 1026-1034.

Verter, V., Kara, B.Y., 2001. A GIS-based framework for hazardous materials transport risk assessment. Risk Anal., 21(6), 1109-1120.

Xie, Q., Ren, J., Huang, H., Fu, K., Zhang, C., Shao, T., 2017. Aging characteristics of epoxy resin discharged by very fast transient overvoltage in SF_6. IEEE Transactions on Dielectrics and Electrical Insulation, 24(2), 1178-1188.

Xue, J., Wang, H., Fan, X., Liu, X., Liu, Y., Li, K., Deng, J.B., Zhang, G., Guo, B., 2018. Surface charge distribution patterns of a truncated cone-type spacer for HVDC GIL/GIS. IET Science, Measurement & Technology.

Yanabu, S., Zaima, E., Hasegawa, T., 2002. Recent development of high voltage circuit breaker for high voltage power transmission and distribution system. Transmission and Distribution Conference and Exhibition, Asia Pacific. IEEE/PES., 2.

Zhang, J., Hodgson, J., Erkut, E., 2000. Using GIS to assess the risks of hazardous materials transport in networks. Eur. J. Oper. Res., 121(2), 316-329.

Zhang, S., Morcos, M.M., Srivastava, K.D., 2017. On the management of metallic particle contamination in gas insulated switchgear. IEEE Transactions on Dielectrics and Electrical Insulation, 24(5), 2746-2754.

Zhang, X., Li, C., Zheng, S., Ji, H., Lu, Q., Wang, Z., 2017. Research of a loop-type sensor embedded in an insulator in 252 kV GIS for partial discharge measurement. 19th International Conference on Mechanical and Intelligent Manufacturing Technologies (ICMIMT), IEEE, 164-173.

How to cite this article: Mastoi, M.S., Nazir, M.S., Chandia, M.I., Khosa, M.S., Nazir, H.M.J., 2018. Optimization of heating characteristics of gas insulated switch-gear (GIS). Scientific Journal of Review, 7(1), 572-590.